Dynamics of Vibrational Overtone Excited Pyruvic Acid in the Gas Phase: Line Broadening through Hydrogen-Atom Chattering

Kaito Takahashi,[†] Kathryn L. Plath,[†] Rex T. Skodje,*[,†] and Veronica Vaida*[,†,‡]

Department of Chemistry and Biochemistry, University of Colorado, Boulder, Colorado 80309, and CIRES, University of Colorado, Boulder, Colorado 80309

Received: April 14, 2008; Revised Manuscript Received: June 2, 2008

The dynamics of overtone-excited pyruvic acid (PA) is studied using a combination of experimental and theoretical methods. It is experimentally observed that high overtone excitation of the OH-stretching mode of PA in the gas phase leads to a unimolecular decarboxylation reaction. An RRKM analysis of the rate is consistent with previous experiments for the thermal reaction but is inconsistent with the present overtone chemistry; from this it is concluded that the overtone-induced reaction is likely to be a direct reaction. Using a Fourier transform infrared spectrometer and a cavity ring-down spectrometer, the spectrum for the OH-stretch fundamental and overtone transitions is measured. We assign two conformers of PA in the spectrum, the Tc and Tt, corresponding to distinct orientations of the OH-group. The spectral peaks for the Tc-conformer broaden dramatically at the third and fourth overtones while those of the Tt-conformer remain relatively narrow. Using a three-mode quantum mechanical model for the vibrational states, the line positions and intensities are well reproduced by theory. The line widths, and the associated dynamical interpretation, are provided by a direct dynamics calculation, where the potential is computed "on-the-fly" and all degrees of freedom are included. It is found that the line broadening is due to the onset of H-atom chattering between the two O-atoms, an effect that occurs for the Tc-conformer but not the Tt-conformer. This H-atom-transfer process is the first step of the decarboxylation reaction mechanism, which subsequently involves breaking the C−C bond. The theoretical and experimental line widths agree but do not correspond to the full reaction time which is much longer than the initial chattering step.

I. Introduction

The vibrational overtone pumping of ground electronic state molecules through direct absorption of infrared or visible light provides an attractive approach to study unimolecular chemical reactions.[1–3] Unlike a thermally induced reaction, chemistry initiated by photon absorption can be investigated over a relatively narrow distribution of internal energy and can, in principle, be treated without the need to explicitly consider the collisional activation process. Although the cross-sections for overtone absorption are small, advances in experimental techniques have permitted the successful study of a number of such reactions including H_2O_2,[4,5] HNO_3,[6] H_2SO_4,[7] N_3H,[8] and HOONO.[9,10] Systems possessing the strong OH-chromophore have proven to be particularly amenable to laboratory studies. A key feature of overtone-induced reactions is that the initial excitation energy is selectively deposited into a specific bright vibrational state, which is often well represented by a vibrational local mode.[11–13] Subsequent intramolecular vibrational energy redistribution (IVR) then leads to energy flow to other modes of the molecule including the reaction coordinate.[14] If the IVR is rapid compared to the unimolecular reaction, one imagines that the excitation is randomized within the active modes of the molecule and a statistical theory such as RRKM theory is appropriate. On the other hand, if the chromophore is strongly coupled to the reaction coordinate, the unimolecular reaction may occur "directly" at a rate far greater than predicted by a statistical theory. There have been numerous attempts to theoretically simulate the intramolecular dynamics of overtone-excited molecules to gain understanding of the fundamental issue of the competition of IVR and reaction.[15–20]

Although the observation of vibrational overtone-induced chemistry can be accomplished through the chemical detection of the reaction products, establishing the associated time scale of the reaction has proven to be a very challenging task for the experimentalists. Direct time-resolved measurements of high-overtone-induced reactions using ultrafast laser technology are scarce at present due to the extremely low absorption cross-sections; however, see Scherer and Zewail.[21] The use of collisional quenching by a variable pressure buffer gas can provide an estimate of the rate, but the results are generally quite approximate because the rates of collisional deactivation are typically not well-known.[22,23] Furthermore, only "slow" statistical reactions can be studied in this way because unrealistically high pressures would be required to study very short-lived species corresponding to direct reactions. Spectroscopic line width analysis provides an alternative approach that does not require knowledge of the collisional energy-transfer rates. If individual molecular eigenstates can be resolved in the spectrum, the line width can ideally be ascribed to lifetime broadening. More commonly, one obtains a broad feature for a bright state that is composed of a sequence of vibrational eigenstates convoluted with the rotational envelope.[11] The homogeneous contribution to the line width can be interpreted as the Fourier transform of an autocorrelation function for the decay of the bright state. It is well appreciated that homogeneous line width provides only an upper bound to the reaction rate,

* Corresponding authors. Electronic mail: R.T.S., Rex.Skodje@colorado.edu; V.V., Veronica.Vaida@colorado.edu.
† Department of Chemistry and Biochemistry.
‡ CIRES.

10.1021/jp803225c CCC: $40.75
Published on Web 07/19/2008

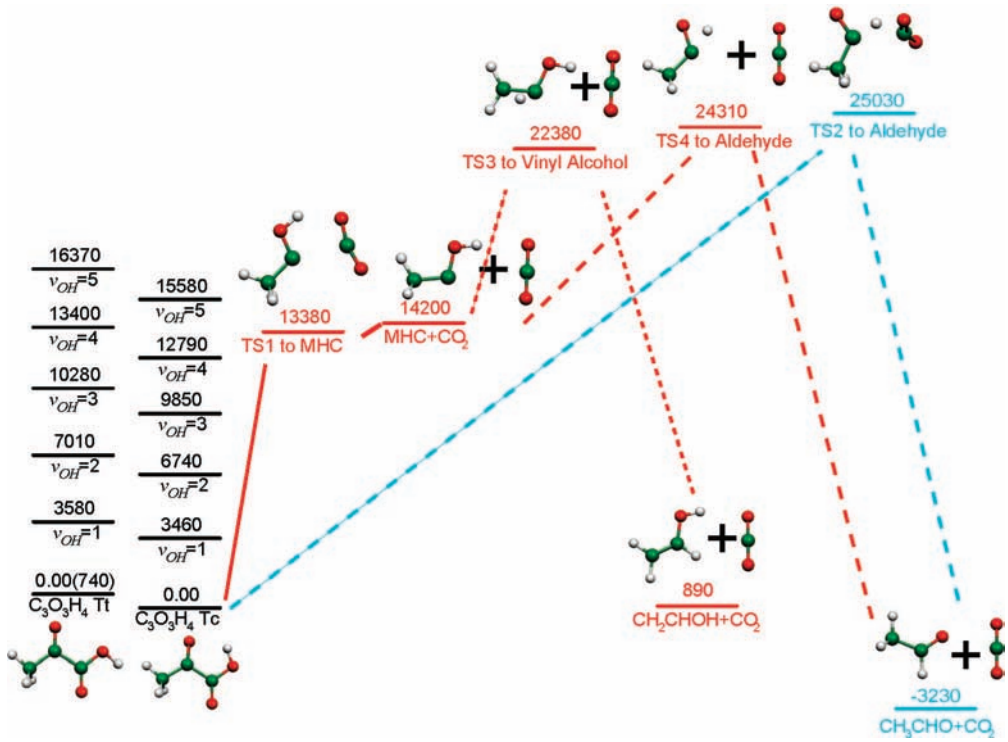

Figure 1. Overview of the decarboxylation pathways of the PA molecule. The relevant transition states (TS) and equilibrium structures have been computed using the B3LYP/6-31+G(d,p) (and confirmed by CCSD(T)/aug-cc-pVTZ//MP2/6-311++G(3df,3pd)) method. The more stable Tc-conformer was found to be most amenable to overtone-induced reaction because of the hydrogen bonded H-atom lying between the donor and acceptor O-atoms. The lowest lying TS1 saddlepoint corresponds to a reaction yielding MHC + CO_2. The higher TS2 saddlepoint yields direct reaction to acetaldehyde + CO_2. The TS3 and TS4 saddlepoint define isomerization pathways to form vinyl alcohol and acetaldehyde, respectively. The energies of the overtone states, shown at the left, suggest that only reaction across TS1 will contribute to the overtone-induced reaction at low temperatures.

$\Gamma_h > \hbar k_r$, because the correlation decay is also influenced (and is often dominated) by the contribution of IVR. Nevertheless, spectral line shape analysis has proven to be a valuable tool to probe the intramolecular dynamics of activated molecules.[4,5,15]

The objective of this study is to investigate the photodecarboxylation reaction of gas phase pyruvic acid (PA), $CH_3COCOOH$, in the ground electronic state by overtone pumping. Unlike most other vibrational overtone initiated reactions studied so far, which occur through the rupture of one bond, the decarboxylation reaction is a concerted process that must involve H-transfer and a C−C bond fission. Furthermore, strong intramolecular hydrogen bonding will be found to play a critical role in the reaction dynamics. Indeed, matrix isolation experiments have revealed the existence of two important conformers, Trans−cis (Tc) and Trans−trans (Tt), which differ dramatically in the degree of hydrogen bonding (see bottom left of Figure 1 for structures). At room temperature, the Tc (with greater hydrogen bonding) comprises ~87% of the population.[24] The present study is of practical importance as well because PA is one of the most abundant ketoacids in the atmosphere where it is generated by photochemical oxidation of biogenically emitted organic compounds (isoprene, cresols). It has been observed in the gas phase, in aerosols, and in rainwater in both the remote continental and marine atmosphere.[25,26] In clouds and aerosols, PA plays a role in secondary organic aerosol formation, which is a process of recent interest because of its effect on climate.[27] The atmospheric importance of this organic acid led to investigations by field measurements, laboratory studies and theoretical modeling. These models included studies of PA's UV photochemistry in the gas phase, in clouds and aerosols, and on ice.[28,29] The main atmospheric loss process for this acid has been conjectured to be UV photolysis.[30] Overtone pumping via the absorption of abundant visible solar photons may provide another loss mechanism as demonstrated for other atmospheric species.[31–36]

The thermal CO_2-elimination process of PA has been thoroughly investigated under a variety of conditions.[37–40] The reaction proceeds readily at elevated temperatures (T > 500 K) but does not occur spontaneously at room temperature. The first step of the mechanism has been conjectured to be CO_2 elimination to form a highly unstable methylhydroxy−carbene[41–43] (MHC) radical with an endothermicity of over 40 kcal/mol. However, as noted by Taylor,[39] the dominant product actually observed is acetaldehyde that is formed with an activation energy of approximately 41 kcal/mol (14300 cm^{-1}).[39,40] From the energetics (presented in Figure 1), it appears quite likely that the reaction proceeds through the MHC intermediate which, then, rapidly isomerizes to form mainly acetaldehyde. Saito et al.[40] have observed a weak absorption signal at 193 nm in a shock tube experiment of PA pyrolysis that was tentatively assigned to a small concentration of the MHC species. For completeness, we note that the UV-photolysis reaction (at wavelengths shorter than 350 nm) has been observed and experimentally characterized.[44–49] Similar to the thermally induced reaction, the dominant products in gas phase UV-photolysis are the low-energy acetaldehyde, or its tautomer vinyl alcohol.

Despite its unique advantages, the vibrational overtone photochemical mechanism has yet to be studied, or even observed, for PA decarboxylation. In this work, we shall examine the dynamics of overtone excited gas phase PA using a combination of experimental and theoretical methods. When the OH-stretching vibration is pumped to the ν_{OH} = 4 and 5 levels, a simple preliminary experiment will establish the basic

fact that the reaction occurs through this mechanism. The main focus of our study is the time-scale of the reaction that will be probed by experimental line shape measurements and a set of dynamical simulations. The time scale of the reaction is quite critical to the fate of an overtone excited PA molecule. Collisions with other gas phase molecules are expected to dissipate the excitation energy, rendering the overtone pumping mechanism ineffective if the unimolecular lifetime is much longer than the mean collision time. The experimental spectra in the regions of the OH fundamental $\upsilon_{OH} = 1$ and overtones $\upsilon_{OH} = 2$, 4, and 5 will be presented. The line widths of the two conformers (Tc and Tt) are found to be dramatically different at $\upsilon_{OH} = 4$ and 5. The dynamics underlying this difference will be theoretically analyzed using a three-mode quantum model for the line positions and intensities of the important bands, along with a direct dynamics simulation of the intramolecular dynamics to obtain the line widths. As one might expect, the dynamics of the two conformers are quite different owing to the distinct orientation of the OH-chromophore. The initial excitation of the Tt-conformer will be found to decay slowly due to a conventional IVR process. In contrast, the excited Tc-conformer exhibits an intriguing dynamical chattering process wherein the H-atom undergoes multiple exchange events between two oxygen atoms. Effectively, this dynamical chattering is the first step of the reaction process that eventually breaks the C−C bond leading to decarboxylation. It is a critical conclusion of this work that the chattering dynamics is responsible for the Tc-line width, corresponding to time-scales on the order of OH-vibrational period, which is much shorter that the overall reaction time. Hence, the line widths do not directly yield the reaction rates but probe the early time processes important in this reaction.

The remainder of this paper will be organized in the following way. In section II, the energetics of the conformers and relevant transition states of PA are computed using quantum chemistry. The rates of thermal decarboxylation reaction are calculated using RRKM theory. The computed rate constants are shown to be in good agreement with experiment but are inconsistent with results for the overtone-induced reaction. From this it is concluded that the overtone reaction is likely to be direct, i.e., nonstatistical. In section III, the experimental and theoretical methods used to study the overtone spectrum are presented. In section IV, the results of experimental measurement and theoretical simulation are presented and discussed. The dynamical simulations are shown to clearly imply that the dynamical chattering of the H-atom is responsible for the dramatic growth in the line width of the Tc-conformer at high excitation. Section V presents our final conclusions.

II. Theoretical Treatment of Electronic Structure and RRKM Rates

In this section, we present a conventional RRKM analysis of the decarboxylation reaction of pyruvic acid based on single point ab initio calculations of the ground state potential and vibrational frequencies. The purpose of this study is two-fold. First, to confirm that we can account for the observed thermal reaction kinetics based on the transition states to the MHC and acetaldehyde products. Second, we wish to estimate the statistical rate constant for the overtone-induced reaction by combining the photon energy with the pre-existing thermal energy of the PA molecule. This rate constant should then provide a lower bound to the homogeneous line width due to reaction. We note in passing that we have performed a preliminary experiment (to be described in a separate publication) that definitely establishes a substantial rate of reaction when the OH-stretch is pumped to $\upsilon_{OH} = 4$ and 5 at room temperature and a total pressure of 630 Torr.[50]

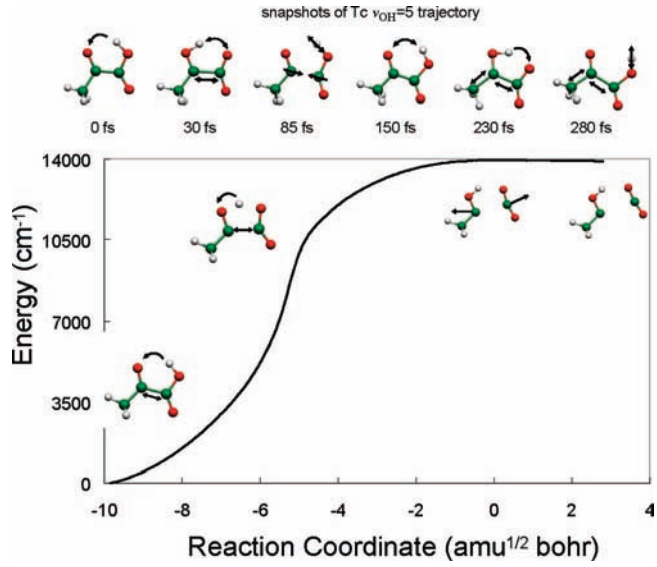

Figure 2. Energy along the minimum energy path (MEP) corresponding to TS1. The MEP follows the B3LYP/6-31+G(p,d) energy from the Tc-equilibrium geometry past the TS1 saddle (at $s = 0$) to product. The TS1 energy is seen to be nearly equal to the product (MHC + CO_2) energy. The molecular structures at various points along the MEP are shown, indicating that the H-atom transfer occurs quickly followed by the C−C bond cleavage. Along the top of the figure are snapshots of direct dynamics trajectory for $\upsilon_{OH} = 5$ of the Tc-conformer that exhibits the H-atom chattering that occur at the early stages of reaction.

We begin with a brief review of the energetics and decarboxylation pathways of highly vibrationally excited PA. The important conformers and transition states are depicted in Figure 1. The equilibrium structures of the conformers of PA and its transition states on the lowest singlet surface were computed using B3LYP[51,52]/6-31+G(d,p)[53–57]and confirmed at the higher CCSD(T)[58–60]/aug-cc-pVTZ[61–63]//MP2[64]/6-311++G(3df,3pd)[53–56] level. We first note that there are two low-energy conformers of PA accessible at room temperature, the Trans-trans (Tt) and Trans−cis (Tc) isomers,[65] that have been observed previously in matrix isolation.[24] The Tc-form is more stable than Tt by 740 cm^{-1} and is characterized by a strong hydrogen bond between the hydroxyl-hydrogen and the ketonic-oxygen atoms. (All energies of the stationary points reported here include the harmonic zero point energy.) The transitions states were found numerically by locating the saddlepoint using the method of Peng et al.[66] such that the maximum component of potential gradient is less that 4.5×10^{-5} au. The lowest transition state, TS1, lies 13400 cm^{-1} above the Tc-PA ground state and is nearly isoenergetic with products MHC and CO_2. The reaction across TS1 consists of a hydrogen-transfer process between the two oxygen atoms followed by the C−C bond cleavage to form MHC + CO_2. The potential energy along the minimum energy path, shown in Figure 2, illustrates that H-transfer is the earliest dynamical step of the reactive process. The reaction proceeds directly from the Tc-conformer but is hindered from the Tt-conformer by a 12.3 kcal/mol adiabatic barrier to internal rotation of the hydroxyl-group. Though these conformers coexist and slowly interconvert at ambient temperatures and pressures, we expect they will exhibit different dynamics. Some of the data obtained for the various transition states using different quantum chemistry methods is shown in Table 1. It is seen that

TABLE 1: Comparison of ab Initio Results for Stationary Points (cm^{-1})

method	ΔE(Tt-Tc)	TS1	TS2	TS3	TS4	TS_{cf}[e]
B3LYP[a]	739	13380	25033	22376	24312	4314
MP2[b]	872	14666	24658	22943	24266	4357
CCSD(T)[c]	915	14200	25816	23045	24825	4270
exp[d]	727					

[a] B3LYP/6-31+G(d,p). All energies include harmonic zero point corrections and are measured from the ground state of the Tc-conformer. [b] MP2/6-311++G(3df,3pd). [c] CCSD(T)/aug-cc-pVTZ//MP2/6-31++G(3df,3pd); MP2 frequencies were used. [d] Experimental value from matrix isolation IR spectra by Riva et al. in ref 24. [e] Transition state for conformational isomerization Tc → Tt.

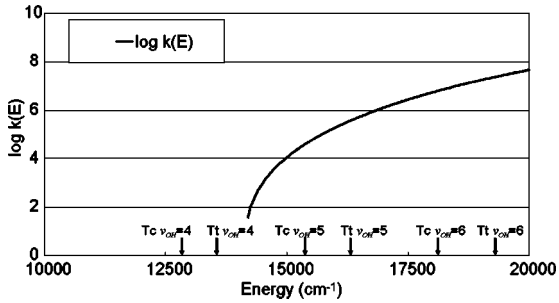

Figure 3. RRKM microcanonical rate constant (s^{-1}) for the reaction PA → MHC + CO_2 versus energy that occurs across the TS1. The excitation energies for the various overtone states are indicated with arrows on the figure.

B3LYP underestimates the barrier for TS1 by about 1000 cm^{-1}; however, the large gap between TS1 and all other transition states is clearly reproduced. These numbers are consistent with previous calculation by Kakker et al.[43]

The observed reaction product in thermal kinetic experiments is dominantly acetaldehyde.[40,45] Any vinyl alcohol produced quickly reverts to the acetaldehyde tautomer. Presumably, a dominant pathway would be to first produce the MHC intermediate through TS1, followed by a second thermal reaction through either TS3 or TS4. Such a mechanism would account for the observed activation energy of 41 kcal/mol because the kinetic measurements monitor the formation of the CO_2 product from the first step. The PA can also directly react to form the more stable acetaldehyde and CO_2 products through the much higher transition state TS2, although this rate is negligible. Also depicted on Figure 1 are the energies of the OH-stretching vibrational overtones of PA under consideration in this study. It is seen that the overtone pumping to $\upsilon_{OH} = 4$ or 5 can only access TS1, the lowest transition state of PA.

Estimates for the RRKM unimolecular rate were made using the energies calculated at the CCSD(T) level along with the frequencies calculated at the MP2 level. The calculations were carried out using traditional methods employing harmonic potentials except for the floppy methyl rotation, which was treated as a free rotor. The mode frequencies for MHC and TS1 are provides in the Supporting Information. The computations were performed using the UNIMOL program suite of Gilbert et al.[67,68]

In Figures 3 and 4 we show the microcanonical rate constant, $k(E)$, and the canonical rate constant, $k(T)$, for the process PA → MHC + CO_2. (We emphasize that the more accurate CCSD(T) energies were used for the RRKM calculations.) In Figure 4, the calculated $k(T)$ for PA decarboxylation (through the TS1 pathway) is presented in comparison with the experimental results reported previously.[38–40] The good agreement

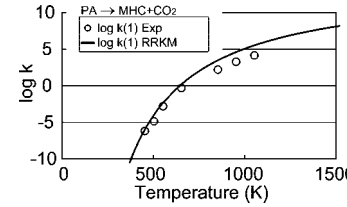

Figure 4. RRKM canonical rate constant for PA → MHC + CO_2 versus temperature (K) computed using TS1. Also shown are the available experimental results for PA loss from refs 39, 40, and 38.

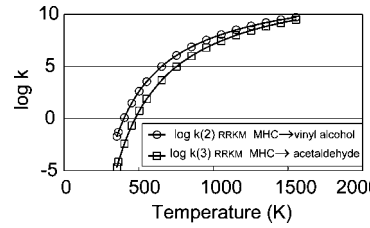

Figure 5. RRKM canonical rate constants versus temperature (K) for the secondary isomerization reactions of MHC to vinyl alcohol and acetaldehyde.

between theory and experiment gives us confidence in the modeling procedure and, in particular, in the accuracy of the ab initio results for TS1. It is also seen that the reaction rate is negligible at room temperature consistent with the known stability of the PA compound. The canonical rate constants for the second step reactions (MHC → acetaldehyde and MHC → vinyl alcohol) are shown in Figure 5. These rate constants are seen to be significantly higher than that for PA → MHC + CO_2. The overall kinetics of the thermal decarboxylation reaction and formation of the final products depends, of course, on the rates of the individual steps PA → MHC + CO_2, MHC → acetaldehyde and MHC → vinyl alcohol. In addition, there can be further reactions of MHC intermediate including the second-order back-reaction MHC + CO_2 → PA. A detailed modeling of the full thermal kinetics is unnecessary in the present work. We do note, however, that at very low PA concentrations the back-reaction is negligible and the first step is rate limiting.

We can use the microcanonical rate constant to make a rough estimate of the statistical rate of reaction expected in the overtone pumping experiment. If the vibrational excitation is rapidly randomized within the molecule, the mean internal energy of the activated PA will be the photon energy plus the mean initial thermal energy (at room temperature) $E = h\nu + \langle E_{thermal} \rangle$. For the experimental conditions,[50] $\langle E_{thermal} \rangle$ is calculated to be roughly 800 cm^{-1} above the zero point energy. The energies of the various overtone states are indicated on the axis of Figure 3. It is seen that the energy of the $\upsilon_{OH} = 5$ overtone state gives a decay rate constant of approximately 10^5 s^{-1}. In contrast, for a direct (nonstatistical) reaction we might expect a far greater rate of decarboxylation following overtone excitation of at least 10^{11} s^{-1} (see below). Under the conditions of the experiment,[50] the hard sphere collision rate of a PA molecule with the buffer gas of N_2 is estimated to be 9×10^9 s^{-1}. It is common for highly vibrationally excited polyatomic molecules at room temperature to transfer at least 100 cm^{-1} per collision in a gas phase environment.[69] Hence, it appears highly likely that if the overtone excitation did randomize within the PA molecule, the initial excitation would dissipate before appreciable reaction could occur. Thus, the observation of reaction at room temperature suggests that the rate is far greater than predicted by statistical theory and is likely direct.

Using the RRKM microcanonical rate constant, it is possible to make a simple estimate of the component of the homogeneous

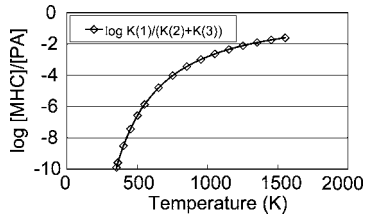

Figure 6. Steady state determination of the concentration ratio [MHC]/[PA] versus temperature (K) for the thermal reaction assuming low initial concentrations of PA so that the back-reaction can be ignored. The steady state concentrations were computed using the PA → MHC + CO_2 rate constant of Figure 4 and the two isomerization rate constants for MHC shown in Figure 5.

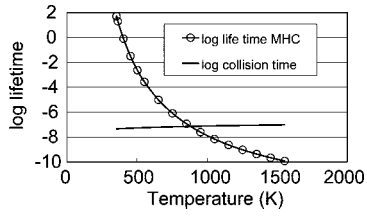

Figure 7. Mean lifetime (s) of a MHC molecule versus T (K) at very low pressure. The lifetime of a MHC molecule is computed by canonical RRKM theory using the rate constants for the secondary reactions shown in Figure 6. Also shown is the mean collision time of MHC in a bath of 1 Torr of PA obtained from a hard sphere collision model.

line width due to reaction. For the scenario of statistical reaction $\Gamma_{rxn} \tilde{} \hbar k(E)$ gives a result of ~0.000001 cm^{-1} for the $\upsilon_{OH} = 5$ overtone excitation. The results presented in section IV reveal a line broadening that is orders of magnitude higher than this estimate, once again suggesting a direct mechanism.

In the thermally induced reaction ($T > 500$ K), the MHC is a transient species that quickly isomerizes to form the final products. We have estimated the concentration of MHC present in a sample as a function of temperature due to thermal chemistry under the conditions of low PA concentrations where the recombination back-reaction can be ignored. Assuming the unimolecular processes PA → MHC + CO_2, MHC → vinyl alcohol, and MHC → acetaldehyde are in steady state, the ratio [MHC]/[PA] versus T is shown in Figure 6. It is clear that the concentration of MHC that might be observed even at 1000 K is only 0.001 of the PA present. This confirms the difficultly of even measuring the MHC species under thermally activated conditions. It is interesting to contrast the thermal kinetics to the results anticipated if the reaction were to proceed through a direct mechanism following overtone excitation at room temperature. Because the photon energy is almost totally consumed by the reaction endothermicity, the nascent MHC would be produced also at roughly ambient temperatures. Thus, the MHC would be quite slow to isomerize and may accumulate a significant concentration. In Figure 7, we show MHC lifetime (computed from the RRKM isomerization rates presented in Figure 4) versus temperature. For comparison, we also plot the collision time for a gas of PA at 1 Torr of pressure. Clearly, the lifetime of ~1 s provides sufficient time for the highly energetic MHC species to undergo potentially important bimolecular reactions such as oligimerization before it reverts to its "uninteresting" isomers.

III. Methods for Studying Overtone Excitation

A. Experiment. The experimental spectra were obtained for gas phase pyruvic acid samples dried using molecular sieves at 0.04 atm at 353 K. The IR spectra between 1000 and 11000 cm^{-1} were obtained in absorption using a Fourier transform infrared spectrometer (FTIR Bruker IFSv/s) at 1 cm^{-1} resolution. These spectroscopic experiments employed a 75 cm cell heated to 353−355 K in an apparatus described in the literature.[70,71] The advantage of this instrument is its wide range of wavelengths covered with very accurate relative intensities. A disadvantage of the FTIR is the low sensitivity, which, together with the decreasing intensity of higher vibrational overtone transitions and low vapor pressure of PA, restricts the use of this instrument to $\upsilon_{OH} \leq 2$. To obtain the sensitivity required to probe the higher overtone transitions near the transition state, a pulsed cavity ring down (CRD) spectrometer, described elsewhere,[72,73,78] was used to provide an expanded effective path length for the spectral region between 12500 and 16700 cm^{-1}. Spectra were collected at a temperature of 355 K with 0.2 and 0.3 cm^{-1} resolution with effective path lengths of 30−50 km depending on the wavelength range.

B. Theory. For the theoretical calculation of the overtone spectra, we calculated the peak positions, absorption intensities (i.e., transition dipole moments), and peak widths. For the calculation of the stick spectrum, we initially assumed the local mode model[74–76] and solved the one-dimensional vibrational problem for the OH-stretching coordinate (R_{OH}) using the method reported previously by one of the authors.[77] However, it was found that this approach compared poorly with the experiment due to large intermode coupling at high-energy excitation. An examination of the "on-the-fly" trajectory simulation (see below) of the excited PA molecule together with a careful analysis of the experimental spectrum suggested that the OH-stretch was strongly coupled to several other normal modes of the molecule. It was determined that the frame bending modes at 252 and 385 cm^{-1} (for Tc) were the most important (depicted in the lower right panel of Figure 8). Therefore, a three-dimensional treatment of the vibrational motion was employed which used the OH-stretch coordinate (R_{OH}) and two normal mode coordinates (Q_{fb1}, Q_{fb2}). The potential energy surface and the vector dipole moment function were computed on a three-dimensional grid of 36000 geometries (40 grid points for R_{OH} and 30 each for Q_{fb} and Q_{fb}) at the Gauss−Hermite quadrature points of (R_{OH}, Q_{fb1}, Q_{fb2}) while holding the remaining normal modes at their equilibrium values. In this way, the full anharmonic potential coupling of these three modes was explicitly included. The vibrational eigenstates were determined using matrix diagonalization of the three-dimensional Hamiltonian. The harmonic oscillator basis set included 20 functions for the OH-stretch and 15 functions for each of the frame bending modes. The intensities of the vibrational transitions from the ground state, and the hot bands from (0,0,1) and (0,1,0), are computed using numerical integration of the dipole function with the converged three-dimensional eigenstates using Gauss−Hermite quadrature. The one-dimensional calculation was performed using the potential energy curve and dipole moment function obtained from B3LYP/6-31+G(d,p), which we have previously found to be reasonably accurate.[78] In addition, the one-dimensional calculation was repeated using a CCSD(T)/aug-cc-pVTZ potential curve to provide an accuracy check on the quantum chemistry. The three-dimensional calculation was performed using only the B3LYP method due to the large grid needed for the calculation.

For the calculation of the full width at half-maximum (fwhm), we assume that each line width, Γ, can be written as the sum of homogeneous and inhomogeneous contributions, $\Gamma = \Gamma_h + \Gamma_i$. The inhomogeneous width is assumed to result primarily from the rotational envelope of the vibrational transition. Making

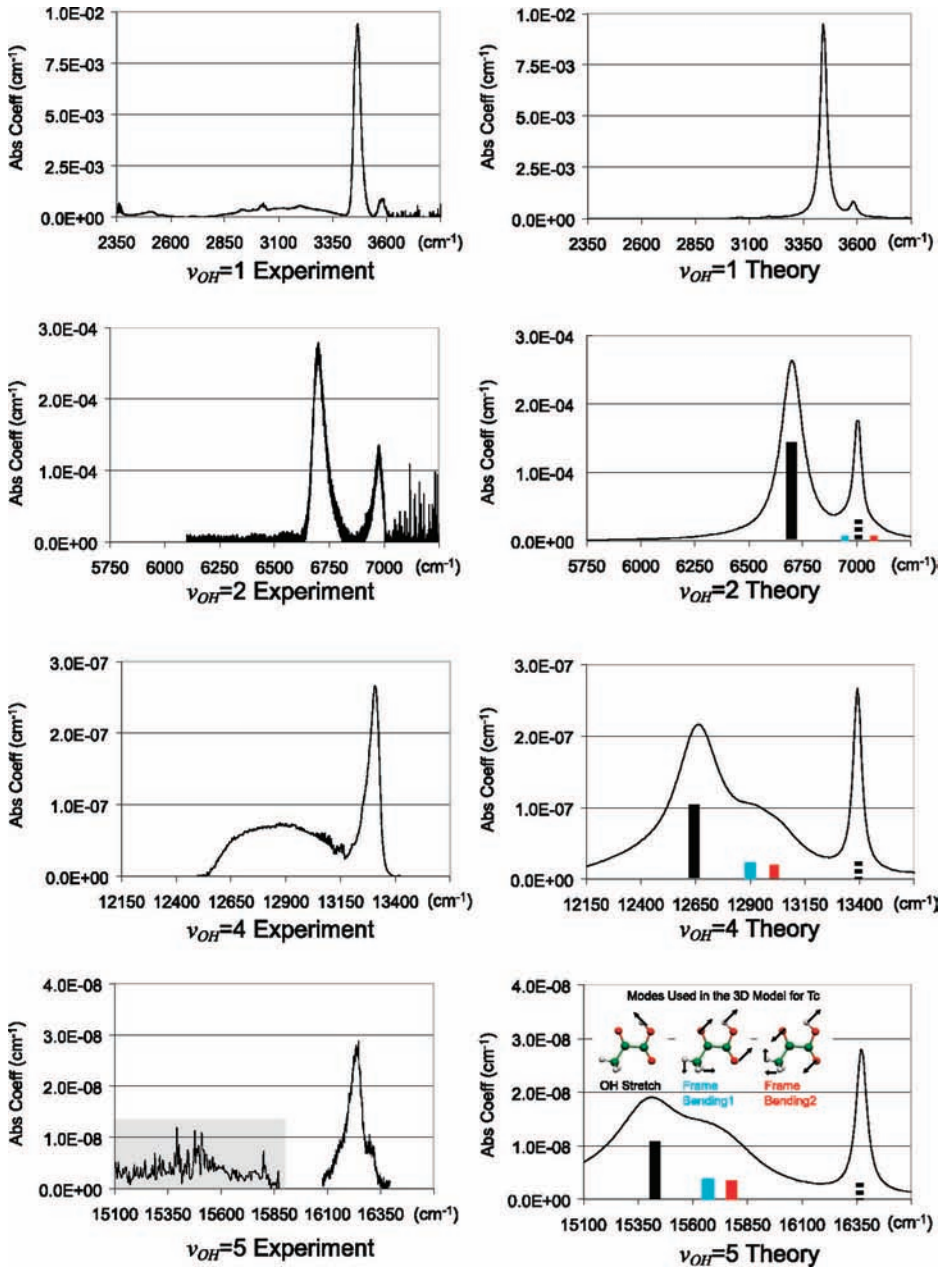

Figure 8. Comparison of experimental and theoretical overtone spectra for PA. The experimental spectra for $\upsilon_{OH} = 1$ and 2 were measured by FTIR spectrometry and the transitions to $\upsilon_{OH} = 4$ and 5 were obtained using CRD spectrometry. The theoretical spectrum was obtained using the three-mode quantum model for the positions and intensities, and the line shapes were Lorentzians with widths composed of a 35 cm^{-1} inhomogeneous component and homogeneous widths computed by direct dynamics simulations. The computed spectrum includes the pure OH-progressions, combination bands, and hot bands involving the frame bending modes. The Tt-peaks (that lie at higher energy) are seen to remain relatively narrow for all overtone transitions, whereas the peaks for the Tc-conformer are seen to broaden dramatically at higher excitations. Stick spectra for the four dominant transitions in the overtone regions are also shown. The solid and dotted black bars signify the pure OH-overtone transitions for Tc and Tt, respectively, and the colored bars signify the combination bands for Tc. The color coding is in accord with the schematic figure of the modes given in the lower left panel.

a symmetric top approximation to the PA molecule, we estimate the inhomogeneous broadening to be about 35 cm^{-1} at 355 K. The homogeneous contributions to the overtone line widths were computed using a classical simulation of the vibrational dynamics employing methods previously developed by us.[79] A separate ensemble of trajectories is created to represent each overtone state in each of the two conformers. The initial conditions are randomly selected on the basis of a one-dimensional model of the OH-stretching mode with zero point energy included in the remaining modes by normal mode sampling. The total energy of each trajectory in the ensemble is fixed at the exact energy of the corresponding overtone state. The coupling to rotational motion of the molecule is ignored ($T = 0$ K, $J = 0$). The trajectories are propagated in the full 24-dimensional space of vibrations, using an "on-the-fly" determination of the potential at the B3LYP/6-31+G(p,d) level that employs analytical Hessians with the propagation method of Hase and Schlegel.[80] The trajectories were propagated for about 200 fs at five-figure accuracy for energy conservation. Small batches of 25−100 trajectories were sufficient to obtain the autocorrelation functions to reasonable accuracy, ∼15%. The homogeneous line widths were computed from the ensembles of trajectories using a classical representation of the autocorrelation function, $\langle\phi(0)|\phi(t)\rangle$, where $\phi(0)$ represents the local mode excitation of

TABLE 2: Peak Positions and Widths from Experiment and Theory

	Tc-conformer				Tt-conformer			
	Frequencies (cm^{-1})		fwhm (cm^{-1})		Frequencies (cm^{-1})		fwhm (cm^{-1})	
v_{OH}	exp	theory	exp	theory	exp	theory	exp	theory
1	3467	3445	37	35	3579	3583	64[a]	35
2	6696	6702	69	79	6975	7007	71	39
4	12920[b]	12663	414	248	13311	13394	56	46
5		15401		366	16237	16375	78	59

[a] Additional broadening of several experimental Tt-peaks occurs due to overlap with the combination states from Tc and overtone states of the CO-stretch. [b] It is difficult to determine the precise $v_{OH} = 4$ experimental peak position for the Tc-conformer because of the broad line shape. The value position reported is the frequency of the highest intensity.

the OH-chromophore. In this representation, the total energy of the local mode OH-stretch was computed versus time. The correlation was computed by the fraction of trajectories remaining within the histogram energy bin of the initial overtone state as the ensemble evolves.[20,15,16] The autocorrelation function was fit to an exponential function to obtain the decay time, and Γ_h is obtained from Heisenberg's uncertainty principle. A Lorentzian function with fwhm of $\Gamma = \Gamma_h + \Gamma_i$ was used to model each peak.

Finally, to obtain a complete spectrum including both conformers, it is necessary to take into account the thermal populations of the Tt- and Tc-conformers of PA at 355 K. From the energetic minimum and the normal-mode frequencies, the populations of the two conformers were extracted. The final spectrum is then obtained by combining the individual spectra for Tt and Tc in proper proportion. We note that the contributions from the vibrational hot-bands of the two frame bending modes have been included in a consistent way in the final results.

IV. Results and Discussion

A. Experimental Spectra. The experimental spectra obtained are shown in the left-hand panels of Figure 8. In the uppermost panel, we show the FTIR scan in the range 2350−3850 cm^{-1} that corresponds to the fundamental transition of the OH-stretch. The spectrum consists of two narrowly split features, i.e., an intense peak at 3470 cm^{-1} and a smaller peak at 3580 cm^{-1}, and background that has been assigned to water impurity. Consistent with previous studies, we have assigned the (larger) low-energy peak to the hydrogen bonded Tc-conformer, and the high-energy peak to the Tt-conformer. The peak width for Tc is measured to be roughly 35 cm^{-1}, and that for Tt is slightly larger due to overlap with other transitions. The experimental positions and widths of the peaks are given in Table 2. The second spectrum probes the first overtone ($v_{OH} = 2$) of the OH-stretch. It is seen that the two primary features persist, although the splitting and relative intensity have changed significantly. The integrated intensity for the smaller Tt-conformer has grown to roughly one-third that of the Tc-conformer (1/8.5 in the fundamental). The second overtone ($v_{OH} = 3$) was inaccessible with the available instrumentation. The third overtone ($v_{OH} = 4$) spectrum shows a dramatic change. The lower energy peak has drastically broadened to roughly a fwhm of 400 cm^{-1} while the higher energy peak remains relatively sharp. The fourth overtone ($v_{OH} = 5$), presented as two separate scans from the CRD spectrometer, reveals even more extreme broadening of the lower energy peak. The low-energy peak region of this overtone was hard to quantify as a peak (thereby given with a gray box in Figure 8); however, absorption was clearly seen for this very broad energy range.

The evolution of the peak splitting between the two conformers with increasing quantum number is not unexpected. Small differences in the vibrational frequencies and anharmonicities of distinct conformation states of a molecule are routinely observed. However, the huge changes in peak widths and, especially, the large difference in the widths between the conformers that develops as v_{OH} increases, bears comment. For the fundamental transition, the peak widths are roughly equal at 35 cm^{-1}. Because (as we noted above) a rough estimate of the rotational envelope at $T = 350$ K is 35 cm^{-1}, it is reasonable to assume that the peak widths for the fundamental transitions are dominated by the inhomogeneous contributions. Furthermore, because we do not expect the inhomogeneous contributions to grow with increasing v_{OH}, the broadening may be due to the homogeneous dynamics of IVR and/or reaction. It is important to emphasize that the Tc-conformer, whose peak undergoes the most extensive broadening, is characterized by the strongest internal hydrogen bonding. The Tc-conformer is also the species most likely to undergo the decarboxylation reaction because the OH-group is properly oriented for the H-atom-transfer process.

One may also speculate that combination bands may develop within the broad low-energy Tc-peaks. This would be consistent with the clear non-Lorentzian line shapes for the $v_{OH} = 4$ and 5 Tc-features. In contrast, the Tt-feature does appear to be roughly Lorentzian. However, we note that the extremely broad $v_{OH} = 5$ "peak" for Tc does not appear to exhibit clear internal structure. This suggests that even if combination transitions are involved, the homogeneous broadening may still be quite large. Finally, we note that the $v_{OH} = 4$ line width of 400 cm^{-1} is converted to time scale for decay of correlation, we obtain $\tau \sim$ 13 fs, which is on the order of an OH-stretch period.

B. Theoretical Stick Spectrum. In Table 3, we present theoretical predictions for the peak positions and intensities computed using the three-dimensional model for the vibrational dynamics. Shown are the results for the pure OH-excitations, (v_{OH}, v_{fb1}, v_{fb2}) = (v_{OH}, 0, 0), and the pertinent combination bands, (v_{OH}, 1, 0) and (v_{OH}, 0, 1). Intensities are given in units of km/mol in base e and can be converted to cm/molecule or dimensionless oscillator strength by the multiplication of 1.66×10^{-19} or 1.87×10^{-7}, respectively. The resulting stick spectrum is plotted in Figure 8. As an accuracy check on the quantum chemistry calculations, we have also computed the line positions of the pure overtone transition using a simple one-dimensional model of the OH-stretch at two levels of theory. It is seen in Table 4 that B3LYP (which is used out of necessity for the 3D calculation) is in reasonable agreement with the more accurate CCSD(T) method. In particular, the crucial splitting of the Tc- and Tt-lines are modeled well by the more approximate BY3LP method.

It is important to note that the combination bands are an important contribution to the spectrum at higher levels of excitation, although they do not significantly affect the funda-

TABLE 3: Peak Positions and Integrated Absorption Intensities Calculated by the 3D Model (B3LYP/6-31+G(d,p))

modes			Tc		
OH	FB1	FB2	peak (cm^{-1})	int abs (km/mol)	comb/pure (%)[a]
1	0	0	3445	1.18E+02	
1	0	1	3697	2.44E−01	0
1	1	0	3830	3.47E−01	0
2	0	0	6702	3.16E+00	
2	0	1	6953	1.36E−01	4
2	1	0	7084	1.33E−01	4
3	0	0	9774	2.00E−01	
3	0	1	10025	1.96E−02	10
3	1	0	10152	1.99E−02	10
4	0	0	12663	1.55E-02	
4	0	1	12916	2.76E−03	18
4	1	0	13038	3.13E−03	20
5	0	0	15401	1.59E−03	
5	0	1	15655	4.37E−04	27
5	1	0	15774	5.61E−04	35
modes			Tt		
OH	FB1	FB2	peak (cm^{-1})	int abs (km/mol)	comb/pure (%)
1	0	0	3583	6.81E+01	
1	0	1	3832	5.94E−03	0
1	1	0	3970	1.77E−02	0
2	0	0	7007	5.39E+00	
2	0	1	7254	9.80E−04	0
2	1	0	7392	4.60E−04	0
3	0	0	10275	3.09E−01	
3	0	1	10521	4.77E−04	0
3	1	0	10660	2.53E−04	0
4	0	0	13394	2.59E−02	
4	0	1	13637	9.86E−05	0
4	1	0	13777	4.08E−05	0
5	0	0	16375	2.97E−03	
5	0	1	16617	1.87E−05	1
5	1	0	16758	6.34E−06	0

[a] The ratio of the intensities of the combination bands to that of the pure overtone transition.

TABLE 4: Peak Positions (cm^{-1}) Calculated by the 1D Model

	B3LYP/6-31+G(d,p)		CCSD(T)/aug-cc-pVTZ	
mode OH	1D (Tc)	1D (Tt)	1D (Tc)	1D (Tt)
0	0 (1798)[a]	0 (1860)	0 (1801)	0 (1860)
1	3457	3585	3466	3593
2	6739	7011	6759	7028
3	9849	10282	9881	10307
4	12794	13402	12836	13432
5	15577	16374	15630	16407

[a] The anharmonic zero point energies are given in parentheses.

mental transition. For $v_{OH} = 2$, the combinations (2,0,1) and (2,1,0) for the Tc-conformer are seen to actually overlap the (2,0,0) peak for the Tt-conformer. However, for the higher $v_{OH} = 4$ and 5 overtones, the combination bands shift away from the Tt-peak and contribute to the wide Tc-feature. It is clear from Table 3 that the combination bands originating from the Tt-conformer have intensities less than 1% of that for the pure overtones and do not significantly contribute. We also point out that hot bands (i.e., transitions from the (0,1,0) and (0,0,1) initial states) also make some contribution to the spectrum and have been included in Figure 8.

It is interesting to compare the line positions predicted by the 1D and 3D models computed at the same B3LYP level of quantum chemistry. It is seen from the tables that the fundamental transition remains nearly the same for both conformers in the 1D and 3D treatments. However, the $v_{OH} = 5$ overtones of the Tc-conformer are red-shifted by ~150 cm^{-1} in the 3D calculation compared to the 1D result. In contrast, the overtones remain the same for the Tt-conformer. Apparently, the OH-stretch of the highly hydrogen bonded Tc-conformer is much more coupled to the frame bending modes than the Tt-conformer. Furthermore, the large coupling also affects the intensity ratio between the combination bands versus the pure overtones. In the Tc-conformer this ratio is ~1:1000 for the fundamental transition, and it drastically increases to 1:3 for the $v_{OH} = 5$ transition (Table 4 column 6). It should be noted that in the Tt-conformer this ratio is still small ~1:100 even at the $v_{OH} = 5$ transition. The overtone stick spectra of the four dominant transitions are shown in the right-hand panel of Figure 8. The solid black bar signifies the pure overtone, and the two colored solid bars represent the two frame bending combination bands for the Tc-conformer. The dotted black bar signifies the pure overtone of the Tt-conformer. Looking at these intensity ratios for $v_{OH} = 4$, 5, it is obvious that if the Tc-conformer had similar widths as Tt, we would see a more structured spectrum with three peaks instead of the large broad peak that is actually observed.

C. Comparison of the Experimental versus Calculated Spectra and Inclusion of the Line Widths. To make a comparison of the theoretical results to the experimental spectrum, the line widths must be included. Thus, each important transition is represented by Lorentzian line shape with an integrated intensity equal to the calculated value. The widths are represented as the sum $\Gamma = \Gamma_h + \Gamma_i$ where Γ_i is taken as 35 cm^{-1} for all transitions. As previously described, the homogeneous widths, Γ_h, are computed from an exponential fit to the correlation decay computed by direct dynamics separately for each transition. The correlation decays for several states are shown in Figure 9. As expected, the stable (reactive) Tc-conformer consistently exhibits a more rapid energy flow out of the OH-stretch. The direct dynamics simulations reveal that decay constants for the stable Tc-conformer are τ (fs) = (120, 24.8, 15.9) for v_{OH} = (2,4,5) and the corresponding lifetimes for the unstable Tt-conformer are τ (fs) = (1406, 468, 222). Using the uncertainty principle, we obtain homogeneous widths of 43.8, 213, 332 cm^{-1} for the Tc-conformer and 3.75, 11.3, 23.9 cm^{-1} for the Tt-conformer, respectively. It is clear that the distinction in the line widths of the two conformers reflects a major difference in the intramolecular dynamics.

In the right-hand panels of Figure 8, we present the theoretical spectra obtained using the width calculated from the direct dynamics autocorrelation functions. It is seen that the theoretical predictions are in reasonably good agreement with observation. For the fundamental transitions, the large peak is confirmed to be the OH(1←0) transition of the stable Tc-conformer and the smaller peak is the same transition of the unstable Tt-conformer. Combination bands are unimportant in this case. The difference in peak heights (about 1:7) is due mostly to relative thermal populations of the two species and the computed intensities are similar; i.e., the intensity for Tc is about 1.5 times that of the Tt. We note that intramolecular hydrogen bonded Tc-conformer exhibits a much smaller intensity enhancement of the OH-stretch fundamental than is usually seen for intermolecular hydrogen bonded complexes. It is likely that the large deviation of the O−H−O angle from the optimal 180° value in the Tc-conformer is responsible for the weak enhancement.[81,82] For the first overtone, $v_{OH} = 2$, the growth in the predicted peak spacing at higher excitation as well as the ratios of the peak maxima are

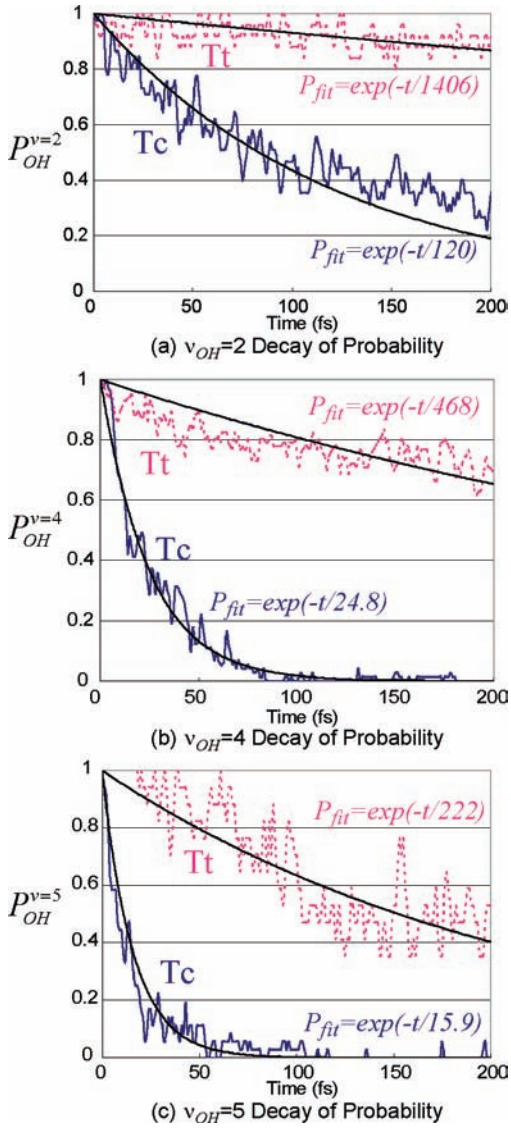

Figure 9. Decay of correlation for the (a) $\upsilon_{OH} = 2$ (b) $\upsilon_{OH} = 4$, and (c) $\upsilon_{OH} = 5$ overtone state of PA. The curves represent the fraction of trajectories of the ensemble remaining within the semiclassical energy bin for the respective υ_{OH} state of the OH-stretch as a function of propagation time. The results for the Tc (blue) and Tt (pink) conformers are shown together. The best fit for an exponential decay curve is also indicated. For $\upsilon_{OH} = 2$ and 5, 50 trajectories and 25 trajectories were used to obtain the ensemble average for Tc and Tt, respectively, whereas for $\upsilon_{OH} = 4$, 100 trajectories each were used to obtain the ensemble average for both Tc and Tt.

likewise in excellent agreement with experiment. The relative increase in the Tt-peak height is mainly due to a greater decrease in the intensity of the overtone from the fundamental of the hydrogen-bonded Tc-conformer (see Table 3). The combination transitions also play a role at this level of excitation, actually increasing the apparent intensity of the unstable conformer. Consistent with experiment, it is seen that the peak width of the stable Tc-conformer increases dramatically at the third and fourth overtones giving a broad feature. In contrast, the peak width for the unstable Tt-conformer grows at a much slower rate. Part of the broadening is due to the growth of the intensity of the combination bands, as mentioned before. However, the dominant broadening mechanism is due to the increase of the homogeneous widths upon high excitation. Although the exact shape is not reproduced, the broad feature in the low-energy side is clearly seen and this is attributed to the great increase in the homogeneous width seen in the Tc-conformer.

TABLE 5: Percentage of Trajectories Exhibiting H-Atom Chattering within 200 fs[a]

B3LYP	quanta	excitation energy (cm^{-1})	H-transfer (%)
Tc	2	6732	0
	4	12770	38
	5	15540	62
Tt	2	7025	0
	4	13435	0
	5	16420	0

[a] A chattering trajectory is identified using the criterion that the distance between the ketonic-oxygen and the hydroxyl-hydrogen atom becomes smaller than 0.97 Å, the equilibrium OH-bond length of product MHC.

Although the overall line widths for the $\upsilon_{OH} = 4$ transition of the Tc-conformer is similar to the experiment, we note that the predicted line shape is somewhat different. Undoubtedly, this is due to limitations in the theoretical model, in particular the elementary model employed for the homogeneous broadening. The classical method used to simulate the (presumed) Lorentzian line widths is a crude approximation to the true quantum dynamics underlying the autocorrelation function. Although we believe the overall time scales obtained for the energy flow were roughly correct, the actual line shapes may be much more complicated than the simple Lorentzian function we assumed. The explicit inclusion of the combination transitions in the spectrum using the lines from 3D quantum model were seen to provide a somewhat more satisfactory representation of the absorption band seen in the experiment. However, we emphasize that in a rigorous treatment of the line shape that the portion of the mode coupling included in the 3D model should then have been eliminated in the determination of homogeneous broadening. Because our motivation was to account for the general trends in the overtone spectrum rather than to reproduce its fine details, such further manipulation was deemed unnecessary.

D. Intramolecular Dynamics of the Excited Molecules. To determine the physical explanation for the unusual spectral differences between the two conformers of PA, we have examined in detail the trajectories generated by the direct dynamics algorithm. The dynamics of the unstable Tt-conformer, at all levels of excitations, were found to be consistent with the usual picture of energy flow in polyatomic molecules. The initial OH-stretch excitation was found to slowly deplete by IVR going mostly into the frame bending and COH-bending modes. The rate of energy flow increased modestly with OH-excitation due to greater mode−mode coupling. In contrast, the dynamics of the stable Tc-conformer are dramatically modified by hydrogen bonding of the OH-group to the ketonic oxygen. For $\upsilon_{OH} = 4$ and 5, it is observed that the hydrogen atom begins to chatter back-and-forth between the two oxygen atoms (see movie given in Supporting Information), similar to other light-atom exchange reactions.[83–93] Essentially, the OH-bond has been broken at these levels of excitations. Conversely, at low levels of excitation, $\upsilon_{OH} = 1$ and 2, the H-atom remains bound to the hydroxyl-oxygen. The rate of energy flow out of the OH-stretch is much less for these lower states. In Table 5, we show the fraction of trajectories within each ensemble that exhibit chattering of the H-atom between the donor and acceptor O-atoms. For $\upsilon_{OH} = 5$, more than half of the trajectories show chattering between the two oxygen atoms. Clearly the broadening of the spectral lines is strongly correlated to the onset of chattering motion.

From our determination of the reaction path, this chattering motion reflects the onset of reactive dynamics across TS1 (the

later portion of the reaction involves cleavage of the C−C bond) as shown in Figure 2. The proximity to the saddlepoint of these trajectories greatly promotes the decay of correlation and massively broadens the associated spectral lines. As the hydrogen atom chatters back and forth between the two oxygen atoms, the C−C bond gradually gains energy eventually causing this bond to break. We emphasize, however, that full reaction to the MHC + CO_2 products was not observed in our simulations for times up to 200 fs. Although the direct dynamics calculations could not be carried out for sufficiently long times to observe appreciable reaction, it is quite clear that the TS1 saddlepoint region is being dynamically accessed. Indeed, "near reactions" with large distensions of the C−C bond were observed. From the rate of energy accumulation in the C−C bond, we estimate the reaction will occur with a rate of at least 10^{11} s^{-1}, far greater than that predicted by statistical theory.

It is a central conclusion of this work that the observed overtone line widths of the Tc-conformer are the result of H-chattering dynamics and not of reaction per se. Indeed, the overall decarboxylation reaction involves breaking two bonds, the O−H and C−C, whereas the line width results from breaking just one. The observed decorrelation time (∼13 fs) and the associated spectral width (∼400 cm^{-1}) are completely understandable in this view because the photon energy is being deposited directly into the O−H bond to be broken.

It is interesting to compare the present reaction of PA to earlier studies of the prototype overtone-induced reaction of hydrogen peroxide, HOOH.[4,5,15,47] In that system, an OH-overtone state was pumped and reaction occurred when energy flowed into the weak O−O bond. Experimental line widths were dominated by inhomogeneous effects,[15] which, unlike the present PA problem, frustrated attempts to extract dynamical information. Furthermore, the theoretical dynamical simulations of the intramolecular dynamics of HOOH revealed that even the homogeneous line widths were dominated by the conventional stretch → bend IVR. It is clear that the PA problem is qualitatively different in that the homogeneous line width reflects the bond breaking process (i.e., H-chattering).

V. Conclusion

In the present work, we have studied the possibility of the overtone-induced decarboxylation reaction of PA though the experimental and theoretical investigation of the OH overtone spectra and reaction kinetics. A preliminary experiment verified that the overtone-induced decarboxylation reaction does occur. An RRKM analysis predicted rate constants in agreement with earlier thermal experiments. However, if the overtone-induced reaction were to proceed statistically, then RRKM theory predicted that the reaction rate would be far slower than the gas phase collision rate. This result strongly suggested that the overtone reaction was dynamically direct, i.e., nonstatistical. It is quite certain that the reaction proceeds through a carbene intermediate (MHC) before proceeding to the acetaldehyde product. The spectrum of PA clearly showed two conformers, the Tc and Tt, for the excitations to $v_{OH} = 1$, 2, 4, and 5. Although the progression for the Tt-conformer behaved in a convention manner (i.e., modest increase in line widths), the peaks for the Tc-conformer exhibited dramatic broadening for the transitions to $v_{OH} = 4$ and 5. The spectrum was reproduced theoretically using a quantum mechanical three vibrational mode model for the peak positions and intensities and a classical direct dynamics simulation of the homogeneous widths. The simulations revealed that combination bands involving low-frequency frame-bending normal modes were important in the high-energy portions of the spectrum. The resulting predicted spectrum was found to be in reasonable agreement with the experimental observations. In particular, the growth of line widths for the Tc-conformer was found to be a homogeneous effect coming from the rapid decay of the OH-bright state. Consistent with experiment, the OH-stretch for the Tt-conformer decayed much more slowly.

It is our central point that the observed broadening of the $v_{OH} = 4$ and 5 overtone peaks of the Tc-conformer is due to the onset of dynamical chattering of the H-atom between the donor and acceptor O-atoms. This chattering behavior is akin to breaking and re-forming the initial OH-bond and results in rapid energy flow occurring on the time scale of the OH-vibrational period. Though the observed line widths do not give the decarboxylation reaction rate, which requires breaking two bonds, it does give the time scale for H-chattering, which is a dynamical precursor to reaction. To our knowledge, the present experiment is the first direct observation of such dynamics using vibrational spectroscopy. Although the time scale of the overall decarboxylation reaction is much longer than vibrational decorrelation time, the simulations and experiment nevertheless suggest that the reaction is direct and proceeds much more rapidly than predicted by statistical theory.

Finally, as a practical matter, we note that the overtone pumping mechanism demonstrated here may lead to very different chemistry for PA than previously observed for thermally initiated reactions. Although elevated temperatures induce MHC production through decarboxylation, they will also isomerize the MHC species to acetaldehyde. In contrast, overtone pumping produces high-energy MHC radicals at ambient temperatures, which are relatively stable. The MHC radicals are thus available for subsequent chemistry through collisions with trace gas phase species. In addition to the back-reaction with CO_2 to re-form PA, a particularly interesting bimolecular reaction would be with water to form ethane diol.

Acknowledgment. V.V. acknowledges support from the NSF. K.P. and K.T. were supported in part by CIRES, University of Colorado. R.T.S. acknowledges support from the Petroleum Research Fund.

Supporting Information Available: The vibration frequencies of the transition state and the MHC radical obtained from quantum chemistry calculations. Two movies of the direct dynamics trajectories for overtone excited PA that show H-atom chattering for the Tc-conformer and conventional IVR for the Tt-conformer. This material is available free of charge via the Internet at http://pubs.acs.org.

References and Notes

(1) Crim, F. F. *Science* **1990**, *249*, 1392.
(2) Crim, F. F. *J. Phys. Chem.* **1996**, *100*, 12725.
(3) Bar, I.; Rosenwaks, S. *Int. Rev. Phys. Chem.* **2001**, *20*, 711.
(4) Butler, L. J.; Ticich, T. M.; Likar, M. D.; Crim, F. F. *J. Chem. Phys.* **1986**, *85*, 233.
(5) Luo, X; Rieger, P. T; Perry, D. S.; Rizzo, T. R. *J. Chem. Phys.* **1988**, *89*, 4448.
(6) Sinha, A.; Vander Wal, R. L.; Crim, F. F. *J. Chem. Phys.* **1990**, *92*, 401.
(7) Vaida, V.; Kjaergaard, H. G.; Hintze, P. E.; Donaldson, D. J. *Science* **2003**, *299*, 1566.
(8) Foy, B. R.; Casassa, M. P.; Stephenson, J. C.; King, D. S *J. Chem. Phys.* **1989**, *90*, 7037.
(9) Konen, I. M.; Li, E. X. J.; Stephenson, T. A.; Lester, M. I. *J. Chem. Phys.* **2005**, *123*, 204318.
(10) Li, E. X. J.; Konen, I. M.; Lester, M. I.; McCoy, A. B. *J. Phys. Chem. A* **2006**, *110*, 5607.
(11) Child, M. S. *Acc. Chem. Res.* **1985**, *18*, 45.

(12) Gruebele, M. *Adv. Chem. Phys.* **2000**, *114*, 193.
(13) Henry, B. R.; Kjaerjaard, H. G. *Can. J. Chem.* **2002**, *80*, 1635.
(14) Miller, Y.; Gerber, R. B. *J. Am. Chem. Soc.* **2006**, *128*, 9594.
(15) Uzer, T.; Hynes, J. T.; Reinhardt, W. P. *J. Chem. Phys.* **1986**, *85*, 5791.
(16) Lu, D.-H.; Hase, W. L. *J. Phys. Chem.* **1989**, *92*, 3217.
(17) Geltino, C.; Sumpter, B. G.; Santamaria, J.; Ezra, G. S. *J. Phys. Chem.* **1989**, *93*, 3877.
(18) Callegan, A.; Srivatava, H. K.; Merker, U.; Lehmann, K. K.; Scoles, G.; Davis, M. J. *J. Chem. Phys.* **1997**, *106*, 432.
(19) Davis, M. J.; Heller, E. J. *J. Phys. Chem.* **1980**, *84*, 1999.
(20) Sibert, E. L., III; Hynes, J. T.; Reinhardt, W. P. *J. Chem. Phys.* **1984**, *81*, 1135.
(21) Scherer, N. F.; Zewail, A. H. *J. Chem. Phys.* **1987**, *87*, 97.
(22) Ravinovitch, B. S.; Flowers, M. C. *Q. Rev.* **1964**, *18*, 122.
(23) Reddy, K. V.; Berry, M. J. *Chem. Phys. Lett.* **1979**, *66*, 223.
(24) Reva, I. D.; Stepanian, S. G.; Adamowicz, L.; Fausto, R. *J. Phys. Chem. A* **2001**, *105*, 4773.
(25) Ervens, B.; Geingold, G.; Frost, G. J.; Kreidenweis, S. M *J. Geophys. Res.* **2004**, *109*, D15205.
(26) Kawamura, R.; Matuura, T. J.; Iizuka, S. *J. Geophys. Res.* **2001**, *106*, 1331.
(27) Carlton, A. G.; Turpin, B. J.; Lim, H.-J.; Altieri, K. E. *Geophys. Res. Lett.* **2006**, *33*, L06822.
(28) Guzman, M. I.; Colussi, A. J.; Hoffmann, M. R. *J. Phys. Chem. A* **2006**, *110*, 3619.
(29) Guzman, M. I.; Hoffmann, M. R.; Colussi, A. J. *J. Geophys. Res.* **2007**, *112*, D10123.
(30) Mellouki, A.; Mu, Y. *J. Photochem. Photobiol. A* **2003**, *157*, 295.
(31) Donaldson, D. J.; Tuck, A. F.; Vaida, V. *Chem. Rev.* **2003**, *103*, 4717.
(32) Matthews, J.; Sinha, A.; Francisco, J. S. *Proc. Natl. Acad. Sci.* **2005**, *102*, 7449.
(33) Staikova, M.; Oh, M.; Donaldson, D. J. *J. Phys. Chem. A* **2005**, *109*, 597.
(34) Miller, Y.; Chaban, G. M.; Finlayson-Pitts, B. J.; Gerber, R. B. *J. Phys. Chem. A* **2006**, *110*, 5342.
(35) Donaldson, D. J.; Frost, G. J.; Rosenlof, K. H.; Tuck, A. F.; Vaida, V. *Geophys. Res. Lett.* **1997**, *24*, 2651.
(36) Wennberg, P. O.; Salawitch, R. J.; Donaldson, D. J.; Hanisco, T. F.; Lanzendorf, E. J.; Perkins, K. K.; Lloyd, S. A.; Vaida, V.; Gao, R. S.; Hintsa, E. J.; Cohen, R. C.; Swartz, W. H.; Kusterer, T. L.; Anderson, D. E. *Geophys. Res. Lett.* **1999**, *26*, 1373.
(37) Weiner, B. R.; Rosenfeld, R. N. *J. Org. Chem.* **1983**, *48*, 5362.
(38) Yamamoto, S.; Back, R. A. *Can. J. Chem.* **1985**, *63*, 549.
(39) Taylor, R. *Int. J. Chem. Kinet* **1987**, *19*, 709.
(40) Saito, K.; Sasaki, G.; Okada, K.; Tanaka, S. *J. Phys. Chem.* **1994**, *98*, 3756.
(41) Yadav, J. S.; Goddard, J. D. *J. Chem. Phys.* **1986**, *85*, 3975.
(42) Matus, M. H.; Nguyen, M. T.; Dixon, D. A. *J. Phys. Chem. A* **2006**, *110*, 8864.
(43) Kakkar, R.; Chadha, P; Verma, D. *Int. Electron. J. Mol. Des.* **2006**, *5*, 27.
(44) Leermakers, P. A.; Vesley, G. F. *J. Am. Chem. Soc.* **1963**, *85*, 3776.
(45) Closs, G. L.; Miller, R. J. *J. Am. Chem. Soc.* **1978**, *100*, 3483.
(46) Davidson, S. R.; Goodwin, D.; Fornier De Violet, P. *Chem. Phys. Lett.* **1980**, *78*, 471.
(47) Buechele, J. L.; Weitz, E.; Lewis, F. D. *Chem. Phys. Lett.* **1981**, *77*, 280.
(48) Rosenfeld, R. N.; Weiner, B. *J. Am. Chem. Soc.* **1983**, *105*, 3485.
(49) O'Neill, J. A.; Kreutz, T. G.; Flynn, G. W. *J. Chem. Phys.* **1987**, *87*, 4598.
(50) To establish the basic fact that vibrational overtone-induced decarboxylation of PA does occur at a reasonable rate, a very simple preliminary experiment was devised. A gas phase sample of PA (PA partial pressure 1.8 Torr) in N_2 in a cell at 630 Torr and 303 K was photolyzed over 3 h at constant temperature with a 1000 W Quartz Tungsten lamp with an intensity of 200 mW/(m^2 nm). Photolysis using a sharp high-energy cutoff at 480 nm, clearly produced CO_2 at a rate of 4.5 × 109 (molecules/min)/cm^3. The production of CO_2 was measured spectroscopically by monitoring the CO_2 band at 2400 cm^{-1} (C═O asymmetric stretch). Under these experimental conditions, the thermal reaction is negligible and the possibility of electronic excitation is precluded. This work will be described in a separate publication.
(51) Becke, A. D. *J. Chem. Phys.* **1993**, *98*, 5648.
(52) Lee, C.; Yang, W.; Parr, R. G. *Phys. Rev.* **1988**, *37*, 785.
(53) McLean, A. D.; Chandler, G. S. *J. Chem. Phys.* **1980**, *72*, 5639.
(54) Krishnan, R.; Binkley, J. S.; Seeger, R.; Pople, J. A. *J. Chem. Phys.* **1980**, *72*, 650.
(55) Clark, T.; Chandrasekhar, J.; Spitznagel, G. W.; Schleyer, P. v. R. *J. Comput. Chem.* **1983**, *4*, 294.
(56) Frisch, M. J.; Pople, J. A.; Binkley, J. S. *J. Chem. Phys.* **1984**, *80*, 3265.
(57) Frisch, M. J.; Trucks, G. W.; Schlegel, H. B.; Scuseria, G. E.; Robb, M. A.; Cheeseman, J. R.; Montgomery, J. A., Jr.; Vreven, T.; Kudin, K. N.; Burant, J. C.; Millam, J. M.; Iyengar, S. S.; Tomasi, J.; Barone, V.; Mennucci, B.; Cossi, M.; Scalmani, G.; Rega, N.; Petersson, G. A.; Nakatsuji, H.; Hada, M.; Ehara, M.; Toyota, K.; Fukuda, R.; Hasegawa, J.; Ishida, M.; Nakajima, T.; Honda, Y.; Kitao, O.; Nakai, H.; Klene, M.; Li, X.; Knox, J. E.; Hratchian, H. P.; Cross, J. B.; Adamo, C.; Jaramillo, J.; Gomperts; R.; Stratmann, R. E.; Yazyev, O. A.; Austin, J.; Cammi, R.; Pomelli, C.; Ochterski, J. W.; Ayala, P. Y.; Morokuma, K.; Voth, G. A.; Salvador, P.; Dannenberg, J. J.; Zakrzewski, V. G.; Dapprich, S.; Daniels, A. D.; Strain, M. C.; Farkas, O.; Malick, D. K.; Rabuck, A. D.; Raghavachari, K.; Foresman, J. B.; Ortiz, J. V.; Cui, Q.; Baboul, A. G.; Clifford, S.; Cioslowski, J.; Stefanov, B. B.; Liu, G.; Liashenko, A.; Piskorz, P.; Komaromi, I. R.; Martin, L. D.; Fox, J.; Keith, T. M.; Al-Laham, A.; Peng, C. Y.; Nanayakkara, A.; Challacombe, M.; Gill, P. M. W.; Johnson, B.; Chen, W.; Wong, M. W.; Gonzalez, C.; Pople, J. A. *Gaussian 03*, revision C.02, Gaussian, Inc.: Wallingford, CT, 2004.
(58) Purvis, G. D., III; Bartlett, R. J. *J. Chem. Phys.* **1982**, *76*, 1910.
(59) Raghavachari, K.; Trucks, G. W.; Pople, J. A.; Head-Gordon, M. *Chem. Phys. Lett.* **1989**, *157*, 479.
(60) Werner, H.-J.; Knowles, P. J.; Lindh, R.; Schutz, M.; Celani, P.; Korona, T.; Manby, F. R.; Rauhut, G.; Amos, R. D.; Bernhardsson, A.; Berning, A.; Cooper, D. L.; Deegan, M. J. O.; Dobbyn, A. J.; Eckert, F.; Hampel, C.; Hetzer, G.; Lloyd, A. W.; McNicholas, S. J.; Meyer, W.; Mura, M. E.; NicklassA. Palmieri, P.; Pitzer, R.; Schumann, U.; Stoll, H.; Stone, A. J.; Tarroni, R.; Thorsteinsson, T. *Molpro, a package of ab initio programs*, version 2002 6; Birmingham, U.K., 2003 (see http://www.Molpro.Net).
(61) Woon, D. E.; Dunning, T. H. *J. Chem. Phys.* **1993**, *98*, 1358.
(62) Dunning, T. H. *J. Chem. Phys.* **1989**, *90*, 1007.
(63) Kendall, R. A.; Dunning, T. H.; Harrison, R. J. *J. Chem. Phys.* **1992**, *96*, 6796.
(64) Moller, C.; Plesset, M. S. *Phys. Rev.* **1934**, *46*, 618.
(65) Yang, X.; Orlova, G.; Zhou, X. J.; Leung, K. T. *Chem. Phys. Lett.* **2003**, *380*, 34.
(66) Peng, C.; Ayala, P. Y.; Schlegel, H. B.; Frisch, M. J. *J. Comput. Chem.* **1996**, *17*, 49.
(67) Gilbert, R. G.; Smith, S. C.; Jordan, M. J. T. *UNIMOL program suite*; 1993.
(68) Gilbert, R. G.; Smith, S. C. *Theory of Unimolecular and Recombination Reactions*; *Blackwell Scientific Publications*, Oxford, 1990.
(69) Hippler, H.; Troe, J.; Wendelken, H. J. *J. Chem. Phys.* **1983**, *78*, 6709.
(70) Luc, P.; Gerstenkorn, S. *Appl. Opt.* **1978**, *17*, 1327.
(71) Richard, E. C.; Vaida, V. *J. Chem. Phys.* **1991**, *94*, 153.
(72) Brown, S. S. *Chem. Rev.* **2003**, *103*, 5219.
(73) Plath, K. L; Takahashi, K.; Skodje, R. T.; Vaida, V. To be published.
(74) Henry, B. R. *Acc. Chem. Res.* **1977**, *10*, 207.
(75) Quack, M. *Annu. Rev. Phys. Chem.* **1990**, *41*, 839.
(76) Henry, B. R.; Kjaergaard, H. G. *Can. J. Chem.* **2002**, *80*, 1635.
(77) Takahashi, K.; Sugawara, M. Yabushita, S. *J. Phys. Chem. A* **2003**, *107*, 11092.
(78) Havey, D. K.; Feierabend, K. J.; Takahashi, K.; Skodje, R. T.; Vaida, V. *J. Phys. Chem. A* **2006**, *110*, 6439.
(79) Takahashi, K.; Kramer, Z. C.; Vaida, V.; Skodje, R. T. *Phys. Chem. Chem. Phys.* **2007**, *9*, 3864.
(80) Millarn, J. M.; Bakkenm, V.; Chen, W.; Hase, W. L.; Schlegel, H. B. J. *Chem. Phys.* **1999**, *111*, 3800.
(81) Howard, D. L.; Jorgensen, P.; Kjaergaard, H. G. *J. Am. Chem. Soc.* **2005**, *127*, 17096.
(82) Filarowski, A; Koll, A. *Vibr. Spectrosc.* **1998**, *17*, 123.
(83) Hiller, C.; Manz, J.; Miller, W. H.; Romelt, J. *J. Chem. Phys.* **1983**, *78*, 3850.
(84) Skodje, R. T.; Davis, M. J. J. *Chem. Phys.* **1988**, *88*, 2429.
(85) Skodje, R. T. J. *Chem. Phys.* **1989**, *90*, 6193.
(86) Cary, J. R.; Skodje, R. T. *Phys. Rev. Lett.* **1988**, *61*, 1795.
(87) Cary, J. R; Skodje, R. T. *Physica D* **1989**, *36*, 287.
(88) Grayce, B. B.; Skodje, R. T. *J. Chem. Phys.* **1991**, *95*, 7249.
(89) Skodje, R. T. J. *Chem. Phys.* **1991**, *95*, 7234.
(90) Grayce, B. B.; Skodje, R. T. J. *Phys. Chem.* **1992**, *96*, 4134.
(91) Grayce, B. B.; Skodje, R. T.; Hutson, J. M. *J. Chem. Phys.* **1993**, *98*, 3929.
(92) Skodje, R. T. *Annu. Rev. Phys. Chem.* **1993**, *44*, 145.
(93) Greaves, S. J.; Kim, J.; Orr-Ewing, A. J.; Troya, D. *Chem. Phys. Lett.* **2007**, *441*, 171.

JP803225C